Islamic Azad University

Journal of

Optoelectronical Nanostructures

Summer 2025 / Vol. 6, No. 1

Research Paper (Pape Type)

High-Performance PCF-Based SPR Sensor for Robust Petroleum Monitoring

Marjan Afshar[1], Mahdi Mehrabi[2*], Mozafaredin Ferdosian Tehrani[3] and Maryam Mohitpour[1]

[1] Department of Electrical Engineering, Shi.C., Islamic Azad University, Shiraz, Iran
[2] Department of Computer Engineering, Shi.C., Islamic Azad University, Shiraz, Iran
[3] Department of Electrical Engineering, Sarv.C., Islamic Azad University, Sarvestan, Iran

Received:
Revised:
Accepted:
Published:

Use your device to scan and read the article online

DOI:

Keywords:
Photonic Crystal Fiber, Pentanol, Amplitude Sensitivity, Surface Plasmon Resonance, Optimization

Abstract:
Accurate detection of petroleum-based compounds like pentanol is vital for quality and efficiency in sectors such as energy and lubrication. Conventional techniques often lack sufficient sensitivity and real-time monitoring capabilities. To address this, we propose a novel photonic crystal fiber (PCF) sensor utilizing surface plasmon resonance (SPR) for precise identification of petroleum compounds, with a focus on pentanol. The sensor incorporates three central apertures to enhance electromagnetic field concentration and employs gold as a durable plasmonic material. Its external analyte positioning not only simplifies fabrication but also ensures robust performance in challenging industrial environments. After thorough optimization of structural parameters including air hole diameter and gold layer thickness the sensor demonstrates a maximum wavelength sensitivity of 9000 nm/RIU and an amplitude sensitivity of 2450 RIU^{-1}, substantially outperforming current alternatives. With its high sensitivity, compact structure, and reliable operation, this sensor is ideally suited for applications such as fuel blending monitoring and quality assurance in the petroleum industry.

Citation: Marjan Afshar, Mahdi Mehrabi, Mozafaredin Ferdosian Tehrani and Maryam Mohitpour.
High-Performance PCF-Based SPR Sensor for Robust Petroleum Monitoring.
Journal of Optoelectronical Nanostructures. 2025; 1 (1): 48-58

***Corresponding author:** Mahdi Mehrabi
Address: Department of Computer Engineering, Shi.C., Islamic Azad University, Shiraz, Iran. **Tell:** 00989177171165 **Email:** mahdi.mehrabi@iau.ac.ir

1. INTRODUCTION

The global economy's reliance on oil remains a cornerstone of modern energy systems, with current demand exceeding 100 million barrels per day. Specifically, as of 2025, global oil consumption is projected to reach approximately 103.5 million barrels per day, reflecting a growth of 0.8 million barrels per day from the previous year [1, 2]. This sustained demand underscores the critical importance of technological advancements in oil production, refining, and monitoring. Innovations in these areas, including advanced refining techniques and leak detection systems, are poised to significantly influence global oil production efficiency and market prices [3]. Consequently, leveraging cutting-edge scientific advancements and technologies in the oil and gas sector is essential for maintaining competitiveness and sustainability [4].

Cost-effective oil production has never been more vital, benefiting not only oil companies and producing nations but also consumer countries that depend on this indispensable resource [5]. Crude oil, primarily composed of paraffinic and aromatic hydrocarbons, yields key petroleum products such as propanol, pentanol, and butane, which are essential for domestic and industrial fuel applications [6, 7]. The precise separation and detection of these compounds are crucial across various industries, driving the demand for advanced sensing technologies. Among these, optical sensors and particularly optical fiber sensors have garnered significant attention due to their accuracy, reliability, and versatility [8].

The future of sensors in chemical and industrial applications is exceptionally promising, having spurred a surge in research and development [9, 10]. A notable breakthrough has been the integration of plasmonic properties with optical sensors, which has led to a marked increase in sensitivity and established surface plasmon resonance (SPR) sensors as a leading technology in sensing applications [11, 12]. Among the most innovative platforms for SPR sensors are photonic crystal fibers (PCFs), which have attracted considerable research interest due to their high compatibility with plasmonic materials [13]. PCF-based SPR sensors offer a range of advantages, including design flexibility, high sensitivity, portability, rapid response, and cost-effective manufacturing, making them ideal for diverse applications [14].

In PCF-based sensors, critical design parameters such as the thickness of the plasmonic layer, the radius and arrangement of air holes, and their spacing play a pivotal role in determining the sensor's performance and sensitivity [15]. In PCF design, circular air holes reduce birefringence compared to angular ones,

whereas rectangular air holes minimize confinement losses by increasing the air filling fraction. Thus, careful selection of air hole shapes allows for simultaneous reduction of birefringence and confinement losses, enhancing overall sensor sensitivity [16]. Optimizing these geometric features enhances the confinement of the electromagnetic field within the fiber core, thereby substantially increasing the sensor's ability to detect changes in the surrounding environment. Plasmon resonance-based optical fiber sensors hold great promise for oil and gas applications, offering rapid detection and high sensitivity [17, 18].

Recent years have witnessed significant growth in research on SPR sensors utilizing PCFs. Advances in plasmonic materials and sensor optimization have expanded their applications across various fields [19]. Prior studies have demonstrated that positioning the analyte outside the sensor and using gold as the plasmonic material facilitate easier fabrication and enhance the coupling between the core and plasmonic modes, resulting in higher sensitivity [20]. Additionally, while D-shaped fibers may offer certain advantages, they are mechanically less robust during manufacturing compared to circular fibers, making the latter more practical for sensor applications [21].

Despite these advancements, challenges remain. Most research on PCF-SPR sensors has focused on enhancing wavelength sensitivity, with less attention given to amplitude sensitivity [22]. Many studies utilize these sensors for detecting high refractive indices (RIs), particularly in the visible to infrared spectrum [23]. However, while PCF-SPR sensors exhibit high sensitivity, their detection range is often limited, hindering their practical utility. Furthermore, confinement loss a key advantage of fiber sensors is heavily influenced by the positioning and geometry of the air holes. Thus, optimizing the arrangement of these holes is crucial for maximizing sensor performance [24].

The persistent challenges of detecting petroleum products with precision and efficiency, vital for industries such as oil and gas, necessitate innovative solutions beyond the constraints of traditional methods. This research introduces a novel PCF-SPR sensor, meticulously designed for pentanol detection, leveraging three central air holes and a gold plasmonic layer to achieve remarkable sensitivities of 9000 nm/RIU for wavelength and 2450 RIU^{-1} for amplitude. As illustrated in Fig. 1, the sensor’s development follows a rigorous, iterative process spanning objective definition, design optimization, simulation, performance assessment, and validation highlighted by a central cross-sectional image of the fiber’s structure. This systematic approach ensures enhanced stability, ease of fabrication, and industrial applicability, promising a

transformative impact on real world petroleum monitoring. Subsequent sections will explore these advancements in greater depth.

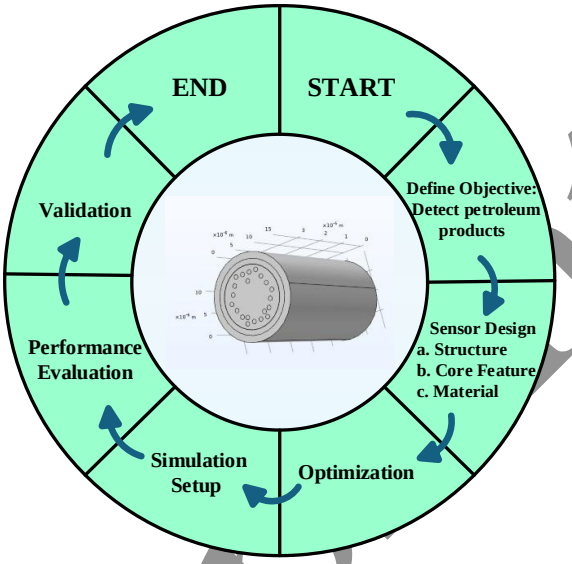

Fig. 1. The proposed iterative development process of the PCF-SPR Sensor for petroleum detection

2. STRUCTURE DESIGN AND THEORY

In the proposed PCF sensor structure, the RI detection range is from 1.31 to 1.4, which has been found suitable for measuring petroleum products. According to Fig. 2, in the design of the proposed optical sensor, triangular air holes have been used as the inner layer, and hexagonal holes have been used as the outer layer in the silica substrate, as well as the gold plasmonic layer. In the design of this sensor, the gold plasmonic layer is considered in such a way that the most concentrated electromagnetic field is placed in the core of the fiber. In addition, the gold plasmonic layer makes this sensor suitable for industrial applications due to its stability in the chemical environment. The central triangle plays an essential role in focusing the electromagnetic field in the fiber core. In the proposed sensor, the analyte is placed outside the sensor, which will lead to the simplicity of the sensor construction. The use of holes around the hexagon reduces the confinement losses and increases the sensitivity of the sensor, and the three central holes play the role of more intense control of the

electromagnetic field in the fiber core. Optimizing the plasmonic layer and the radius of the air holes as well as finding the best placement points of the internal holes based on logical principles are other advantages of this sensor. The internal holes that form the vertices of a triangle with three different angles, including an equilateral triangle with an apex angle of 40 degrees (Fig. 2(d)), an isosceles triangle with an apex angle of 135 degrees (Fig. 2(b)) and an equilateral triangle (Fig. 2(c)) have been investigated to ultimately lead to the intelligent selection of the location of the central holes.

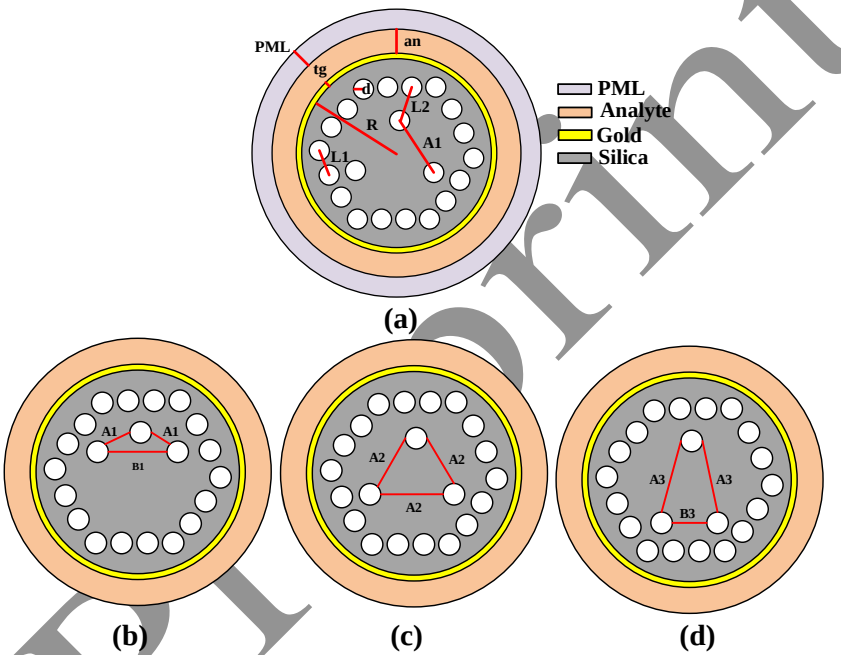

Fig. 2. Designed geometry of the proposed sensor. Schematics of (a) the proposed optical sensor, (b) isosceles triangle with an apex angle of 135 degrees of the internal hole geometry, (c) isosceles triangle of the geometric hole and (d) isosceles triangle with an apex angle of 40 degrees of the internal hole geometry

Table I outlines the optimized design parameters, as depicted in Fig. 2 (a), which define the sensor's structural geometry. These include the perfectly matched layer (PML) thickness of 1.2 µm, the gold plasmonic layer thickness (tg) of 40 nm, the pitch (an) of 1.5 µm, the radius of the central apertures (r) of 7 µm, and the diameter of the lattice air holes (d) of 0.5 µm. Additional parameters, such as L1 = 3.3 µm, L2 = 3.3 µm, A1 = 4.4 µm, A2 = 7 µm, A3 = 9 µm, B1 = 6.74 µm, and B3 = 5.5 µm, further specify the sensor's

configuration. These values are fine-tuned to maximize the sensor's performance, achieving a wavelength sensitivity of 9000 nm/RIU and an amplitude sensitivity of 2450 RIU^{-1}, as highlighted in the study.

The sensor incorporates three central apertures to enhance electromagnetic field focus, with their arrangement optimized through different geometric configurations. Table II compares the amplitude sensitivities of three configurations of these central holes, characterized by their vertex angles. The configuration with a 60-degree vertex angle, illustrated in Fig. 2(c), yields an amplitude sensitivity of 2450 RIU^{-1}, significantly outperforming the 40 & 60-degree configuration, which achieves 512 RIU^{-1} and 786 RIU^{-1} respectively. Due to its superior sensitivity, the 60-degree configuration is selected for all subsequent analyses and reported results.

The overall structure, as shown in Fig. 2(a), features a hexagonal lattice of air holes embedded in a silica matrix, with the analyte positioned externally to simplify fabrication and enhance durability in challenging environments. Figs. 2(b), 2(c), and 2(d) depict variations in the internal hole geometry, where the central holes form isosceles triangles with specific apex angles. Fig. 2(c) corresponds to the 60-degree vertex angle configuration, optimizing the electromagnetic field interaction for enhanced SPR effects. This design ensures the sensor's high sensitivity, compact footprint, and suitability for industrial applications.

TABLE I
THE VALUE OF THE PROPOSED SENSOR PARAMETERS

Parameters name	parameters value
PML	1.2 µm
tg	40 nm
an	1.5 µm
R	7 µm
d	0.5 µm
L1	3.3 µm
L2	3.3 µm
A1	4.4 µm
A2	7 µm
A3	9 µm
B1	6.74 µm
B3	5.5 µm

TABLE Ⅱ
VALUES OF TRIANGLE APEX ANGLES IN THE PROPOSED SENSOR

Fig.2	Vertex angle (degree)	Amplitude sensitivity (RIU^{-1})
b	135	786
c	60	2450
d	40	512

Fig. 3, shows the placement of the proposed sensor in the laboratory setup. The polarized light enters the proposed sensor through a single mode fiber. Around the proposed sensor is a compartment for the entry and exit of the analyte. The analyte is placed on the outer surface of the sensor and the light is emitted from the sensor after reacting with the analyte. The output light is analyzed through a spectrum analyzer and its waveform is displayed on the computer screen. Changes in the output light peak or the displacement of the peaks relative to each other cause the sensing property to occur.

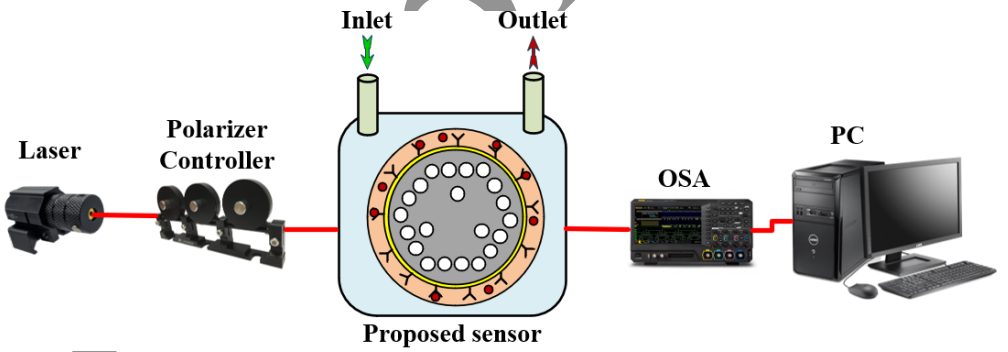

Fig. 3. Sensor setup for sensing application

According to the analysis of the obtained results, the best possible state is in line with the angles of the central holes in the proposed optical sensor, completely symmetrical and with an angle of 60 degrees. This case once again justifies the use of symmetry in the design and manufacture of optical sensors based on photonic crystals. When the central holes form an equilateral triangle, the maximum limitation of the core mode occurs inside the fiber core and increases the sensitivity of the sensor. In Fig. 4, Electromagnetic fields are shown from left to right in core mode (a), coupling mode (b), and plasmonic

mode (c), for polarization in the x direction. Because the polarization in the x and y direction has the same value, it is enough to obtain all the graphs for one of the polarizations.

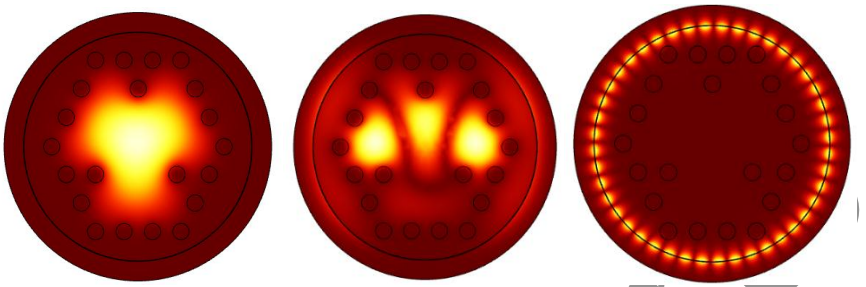

(a) **(b)** **(c)**

Fig.4. Electromagnetic field for (a) core mode, (b) core-plasmonic coupling, and (c) plasmonic mode.

3. MATHEMATICS AND FORMULAS

The proposed sensor is based on silica as its background material. The dispersion relation for silica is derived from the Sell Meier in Eq. (1) [25].

$$n_{si}^2 = 1 + \frac{B_1\lambda^2}{\lambda^2 - C_1} + \frac{B_2\lambda^2}{\lambda^2 - C_2} + \frac{B_3\lambda^2}{\lambda^2 - C_3} \quad (1)$$

where λ measured in μm unit is the related wavelength and n_{si} is the RI of fused silica. B_1, B_2, B_3, are 0.696166300, 0.407942600, 0.897479400 and C_1, C_2, C_3 are, $4.67914826 \times 10^{-3}$ μm^2, $1.35120631 \times 10^{-2}$ μm^2, 97.9340025 μm^2, respectively [26].

The sensor utilizes gold metal as its plasmonic material, enhancing its stability within biological environments. The incorporation of this material significantly influences both the resonance peak and the sensor's detection capabilities. The dielectric function of gold is derived from the Drude-Lorentz model which is formulized in Eq. (2) [27].

$$\varepsilon_{Au} = \varepsilon_{\infty} - \frac{w_D^2}{w(w + j\gamma_D)} - \frac{\Delta\varepsilon\Omega_L^2}{(w^2 - \Omega_L^2) + j\Gamma_L w} \quad (2)$$

where ε_{Au} is the permittivity of the gold and $\varepsilon_{\infty} = 5.9673$ is the permittivity at a high frequency. The rest of the constant parameters in (2) were obtained from

[28]. The efficiency of the sensor is calculated by confinement loss characteristics in Eq. (3)

$$CL = 8.686 \times k_0 \times Im(n_{eff}) \times 10^4 \ (dB/cm) \quad (3)$$

The parameter k0, defined as $2\pi/\lambda$, represents the wave propagation number in free space, where λ denotes the operating wavelength, and Im(neff) refers to the imaginary component of the effective mode index. The sensitivity of the proposed sensor is assessed through wavelength interrogation and amplitude interrogation techniques [29]. The wavelength sensitivity (WS) of the suggested plasmonic sensor is derived from the subsequent equation in Eq. (4) [25]:

$$WS = \frac{\Delta\lambda}{\Delta n_a} \ (nm/RIU) \quad (4)$$

where Δn_a and $\Delta\lambda$ show the RI variation of the two consecutive analytes and the wavelength variation of the resonance peak, respectively. The amplitude sensitivity (AS) of the proposed sensor can be computed from the following relation in Eq. (5) [30]:

$$AS = \frac{-1}{\alpha(\lambda, n_a)} \frac{\delta\alpha(\lambda, n_a)}{\delta n_a} \ (RIU^{-1}) \quad (5)$$

where n_a, $\delta\alpha(\lambda, n_a)$ and $\alpha(\lambda, n_a)$, display dielectric RI, the variation of loss spectrum for two consecutive n_a and confinement loss for any n_a, respectively.

In the proposed sensor, we place significant emphasis on enhancing amplitude sensitivity [31]. Since the amplitude sensitivity does not require spectral manipulation, it makes the proposed sensor simple and efficient [32].

4.RESULTS AND DISCUSSION

The proposed sensor is designed, simulated and optimized in the COMSOL software environment. This software uses the FEM model to solve wave equations and Maxwell's equations inside the structure. According to this model, the problem is divided into smaller parts and based on the meshing of the structure, the corresponding equations are solved for each part. In this structure, after designing the geometry and specifying the dimensions, we have used a very fine mesh to solve the wave equations more accurately. Also, a PML layer is considered to shorten the calculation area in this sensor. Finally, the results

were analyzed by changing the RI of the analyte and the sensing property was extracted from the structure.

The geometry of the proposed PCF sensor has been optimized in a special way, in such a way that the core mode and the plasmonic mode match in it and it has increased the amplitude sensitivity. According to Fig. 5, when the effective RI of the core mode collides with the plasmonic mode, at the point of their intersection, an intensification occurs and a sharp peak of confinement losses occurs. The displacement and intensity of this peak in different RIs is the sensitivity measure of the proposed sensor.

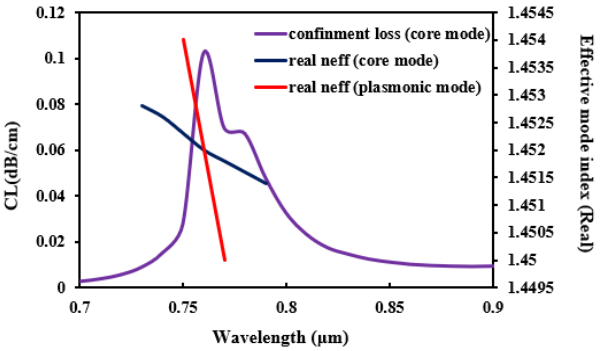

Fig. 5. Electric field distribution for x polarization, core guided mode and SPP mode for na=1.4.

In Fig. 6, The resonant wavelength of the proposed sensor is displayed based on the range of RIs that can be detected by the sensor, and the corresponding equation is written as a polynomial. In the proposed third grade equation corresponding to the behavior of the sensor, the x parameter represents different RIs and the y parameter represents the wavelength in micrometers, according to this equation, the resonant wavelength (RW) of each RI can be determined.

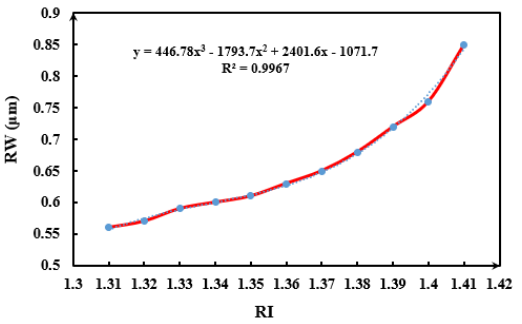

Fig. 6. Linear curve fitting of resonance wavelength

The designed sensor covers a wide range of RIs (RI from 1.31 to 1.41). At the RI of 1.4, the maximum sensitivity of the sensor can be seen. In Fig. 7(a), the amount of confinement losses and the amplitude sensitivity from RI 1.31 to 1.41 are shown. Fig.7(a), shows that the confinement loss increases as the RI increases, and the maximum confinement loss will be at a RI of 1.41. In Fig. 7(b), the amplitude sensitivity is displayed for different RIs, based on this, the highest sensitivity for the RIs of 1.4 and 1.39, respectively, which represents the two substances pentanol and butanol, is equal to the wavelength sensitivity of 9000 nm/RIU and amplitude sensitivity of 2450 RIU^{-1} for pentanol, and wavelength sensitivity of 4000 nm/RIU and amplitude sensitivity of 1400 RIU^{-1} for butanol.

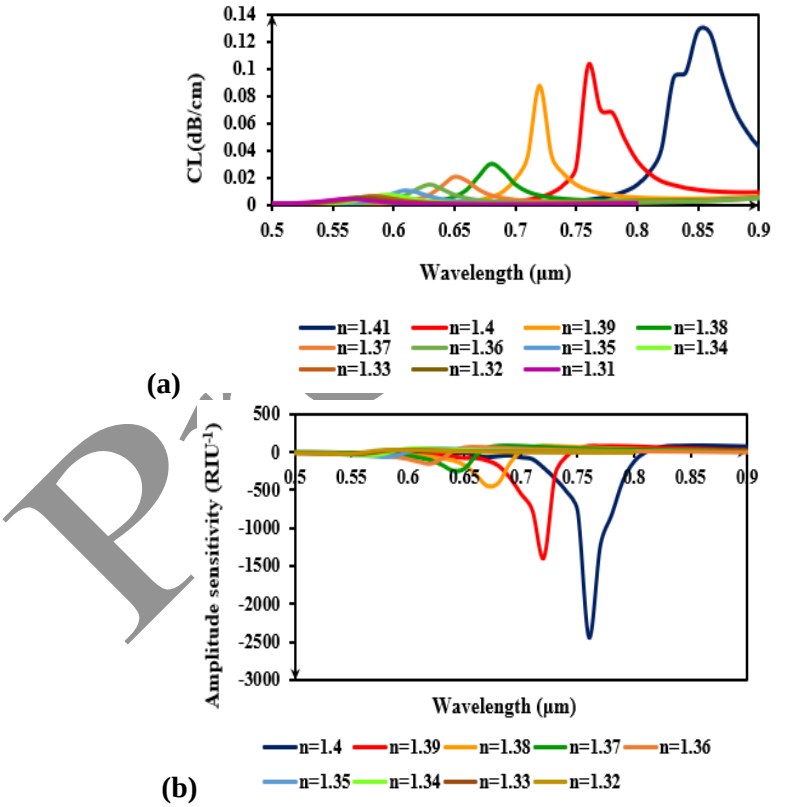

Fig. 7. (a) CL as RI changed from 1.31 to 1.41 and (b) AS spectrum for RI from 1.32 to 1.4.

According to the investigations and optimizations carried out in the design of the proposed optical sensor, in the case that the central air holes are in the form of an isosceles triangle with an apex angle of 40 degrees, the appearance of several peaks next to the main peak causes a disturbance in sensitivity, When analyzing the sensitivity of different placement positions for the internal holes, particularly for the apex angles of 60° and 135°, Fig. 8, demonstrates that the sensitivity of the 60° mode is significantly higher than that of the other two modes.

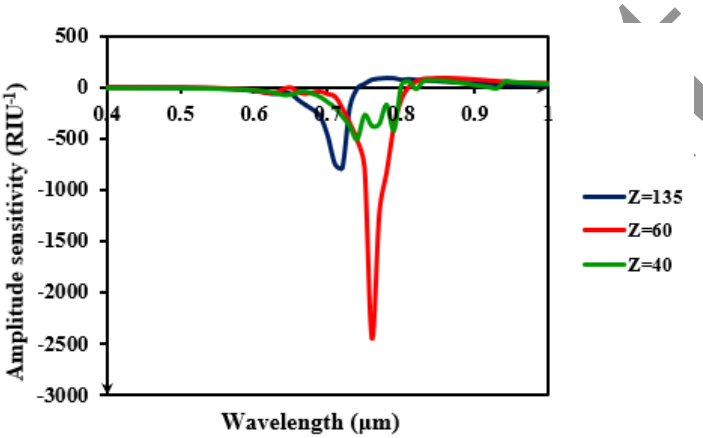

Fig. 8. Change of the tip angle of the internal holes of the proposed PCF sensor

Continuing the optimizations discussed earlier, Fig. 9, illustrates the confinement loss values (Fig. 9a) and amplitude sensitivity (Fig. 9b) as functions of the gold plasmonic layer thickness. Fig. 10, shows the changes of the radius of the air holes, confinement losses (Fig.10(a)) and the amplitude sensitivity (Fig.10(b)). The highest amplitude sensitivity is obtained at a radius of 500 nm and with a value of 2450 RIU^{-1}. If we have a manufacturing tolerance of 0.2 micrometer from the optimal radius of the holes, changes in the value of the amplitude sensitivity can be seen.

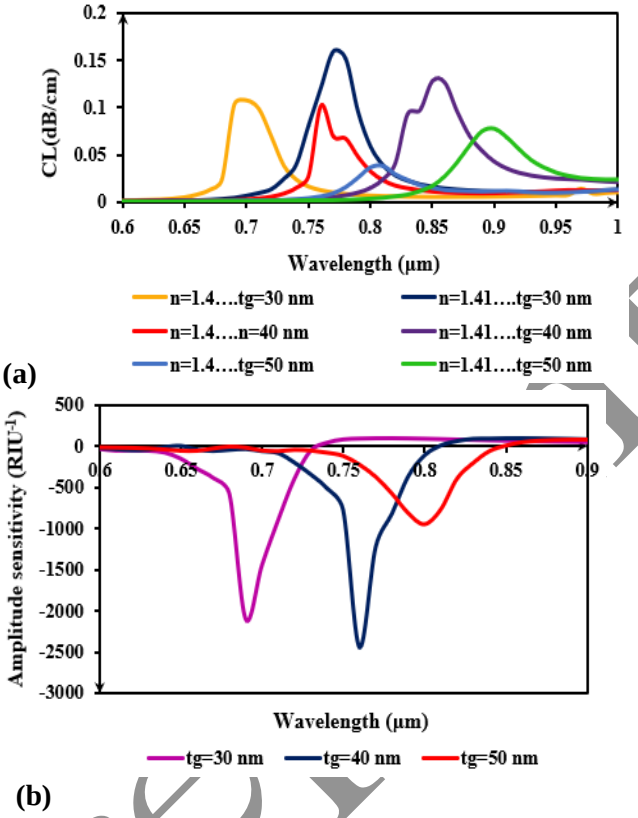

Fig. 9. (a) CL for different gold layer thicknesses and (b) AS for different gold layer thicknesses

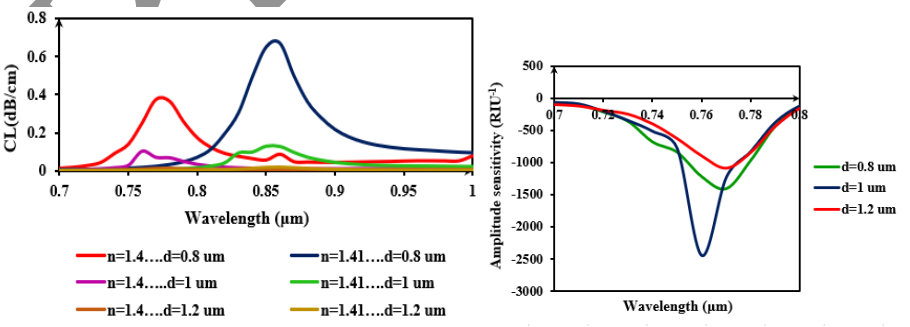

Fig. 10. (a) CL for different air hole diameters and (b) AS for different air hole diameters

Table Ⅲ shows amplitude sensitivity and wavelength sensitivity for different RIs and its application in the oil and gas industry. The RIs covered by the sensor range from 1.31 to 1.41, which is within the range of the RI of oil and gas compounds. By increasing the RI, the amplitude sensitivity and wavelength sensitivity of the sensor increased, and in the RI of 1.4, which is assigned to pentanol, the highest amplitude sensitivity of 2450 RIU^{-1} and the highest wavelength sensitivity of 9000 nm/RIU occur at the resonant wavelength of 760 nm.

TABLE Ⅲ
MEASUREMENT PERFORMANCE OF OIL COMPONENT DETECTION SENSOR FOR DIFFERENT RI

Oil Derivation	Analyte RI	Peak wavelength (nm)	Resonance Peak Shift (nm)	Wavelength Sensitivity (nm/ RIU)	Amplitude Sensitivity (RIU^{-1})
NA	1.31	560	100	1000	54
Methanol	1.32	570	200	2000	55
Water	1.33	590	100	1000	56
Acetonitrile	1.34	600	100	1000	57
NA	1.35	610	200	2000	58.8
Ethanol	1.36	630	200	2000	152
Propanol	1.37	650	300	3000	252
NA	1.38	680	400	4000	403
Butanol	1.39	720	400	4000	1400
Pentanol	1.4	760	900	9000	2450
NA	1.41	850	NA	NA	N/A

To facilitate a comprehensive comparison of the proposed optical sensor with existing structures in the field, Table Ⅳ is presented. The proposed sensor, a PCF with three central air holes, operates over a wavelength range of 400 nm to 1100 nm, covering a significant portion of the visible and near-infrared spectrum. This broad range is particularly advantageous for applications such as detecting petroleum-based compounds like pentanol, which exhibit refractive indices within the measurable range of 1.31 to 1.41. In terms of sensitivity, the proposed sensor achieves a wavelength sensitivity of 9000 nm/RIU, which is comparable to some of the highest reported values in recent literature. More notably, the amplitude sensitivity of the proposed sensor stands at 2450 RIU^{-1}, surpassing that of most listed sensors. This high amplitude sensitivity is particularly beneficial for applications requiring precise detection of small

refractive index changes.

Beyond its sensitivity, the proposed sensor's design is characterized by simplicity and flexibility. The use of three central air holes allows for straightforward fabrication processes, reducing complexity and cost. Additionally, the design permits easy adjustment of structural parameters, such as hole diameter and spacing, to optimize performance for specific applications. This adaptability, combined with its robust performance, makes the sensor highly practical for real-world implementation. In summary, while the proposed sensor may not hold the record for the highest wavelength sensitivity, its combination of broad operational range, high amplitude sensitivity, and design simplicity positions it as a competitive and versatile tool for refractive index sensing, particularly in the context of petroleum compound detection.

TABLE Ⅳ
PERFORMANCE COMPARISION OF THE PROPOSED SENSOR WITH RECENTLY REPORTED RI SENSORs

Structure Type	Wavelength range (nm)	RI Range	Wavelength sensitivity (nm/RIU)	Amplitude sensitivity (RIU^{-1})	Ref
Hollow core PCF	500-900	1.33-1.38	3100	NA	[33]
Asymmetric multiple holes-PCF	400-950	1.32-1.41	9000	1540	[34]
D-shaped hollow micro structured-PCF	NA	1.3-1.39	9900	425.58	[35]
D-shaped-PCF	NA	NA	3700	1789	[36]
Nano-layer coated-PCF	400-1200	1.31- 1.41	21000	2127.7	[37]
Dual core-PCF	1400-2600	1.1-1.45	24300	172	[38]
Hoop-cut SPR PCF	NA	1.39-1.44	2000	374	[39]
Dual‐side polished SPR PCF	560-1860	1.21-1.41	61000	1294	[11]
Three central air holes PCF	400-1100	1.31-1.41	9000	2450	This paper

5. Conclusion

In this paper, we design and present a PCF sensor based on SPR. The proposed sensor offers high sensitivity and is easily manufactured for detecting petroleum compounds, particularly pentanol and butanol. The incorporation of a gold plasmonic layer enhances its stability in chemical and industrial environments. Additionally, the use of air holes in a triangular configuration enhances the concentration of the electromagnetic field at the fiber's center using the minimum number of holes. Optimized geometric parameters and air hole placement yield significant improvements, with the sensor achieving peak wavelength sensitivity of 9000 nm/RIU and amplitude sensitivity of 2450 RIU^{-1} for pentanol, respectively. This performance surpasses that of other sensors in the field. The sensor's stability, compact size, flexibility, simple design, and high sensitivity instill confidence in its practical application for detecting petroleum compounds. These attributes position it as a promising advancement for industrial use, warranting further exploration in future studies.

References

[1] Kumhof, M. and D. Muir, Oil and the world economy: some possible futures. Philosophical Transactions of the Royal Society A: Mathematical, Physical and Engineering Sciences, (2014). 372(2006): p. 20120327. Available:https://royalsocietypublishing.org/doi/abs/10.1098/rsta.2012.0327

[2] Hosseini, S.H., H. Shakouri, and A. Kazemi, Oil price future regarding unconventional oil production and its near-term deployment: A system dynamics approach. Energy, (2021). 222: p. 119878. Available:https://www.sciencedirect.com/science/article/abs/pii/S0360544221001274

[3] Meribout, M., et al., Leak detection systems in oil and gas fields: Present trends and future prospects. Flow Measurement and Instrumentation, (2020). 75: p. 101772. Available: https://www.sciencedirect.com/science/article/abs/pii/S0955598620301205

[4] Guangjie, Y., et al., The up-to-date drilling and completion technologies for economic and effective development of unconventional oil & gas and suggestions for further improvements. Petroleum Drilling

Techniques, (2022). 50(1): p. 1-12. Available: https://www.syzt.com.cn/en/article/Y2022/I1/1

[5] Awogbemi, O. and D.V. Von Kallon, Achieving affordable and clean energy through conversion of waste plastic to liquid fuel. Journal of the Energy Institute, (2023). 106: p. 101154. Available: https://www.sciencedirect.com/science/article/abs/pii/S1743967122002021

[6] Yolchuyeva, U., et al., Investigation of Surakhani light crude oil compounds as a case study using modern spectroscopic techniques. Journal of Petroleum Exploration and Production Technology, (2024). 14(1): p. 289-302. Available: https://link.springer.com/article/10.1007/s13202-023-01702-6

[7] Kim, J., et al., Analytical methods for detecting butane, propane, and their metabolites in biological samples: Implications for inhalant abuse detection. Journal of Chromatography B, (2024). 1234: p. 124011. Available: https://www.sciencedirect.com/science/article/abs/pii/S1570023224000199

[8] Robson, W.J., et al., Class type separation of the polar and apolar components of petroleum. Analytical chemistry, (2017). 89(5): p. 2919-2927. Available: https://pubs.acs.org/doi/abs/10.1021/acs.analchem.6b04202

[9] Fallahi, V., M. Hosseini, and Z. Kordrostami, Optimization of highly sensitive three-layer photonic crystal fiber sensor based on plasmonic. Physica Scripta, (2024). 99(10): p. 105577. Available: https://iopscience.iop.org/article/10.1088/1402-4896/ad7cd7/meta

[10] Fallahi, V. and M. Seifouri, Novel four-channel all optical demultiplexer based on square PhCRR for using WDM applications. Journal of Optoelectronical Nanostructures, (2018). 3(4): p. 59-70. Available:https://www.researchgate.net/profile/VahidFallahi/publication/330936584_Novel_FourChannel_All_Optical_Demultiplexer_Based_on_Square_PhCRR_for_Using_WDM_Applications/links/5c5c6872299bf1d14cb33cad/Novel-Four-Channel-All-Optical-Demultiplexer-Based-on-Square-PhCRR-for-Using-WDM-Applications.pdf

[11] Khodatars Dashtmian, M.R., et al., Highly sensitive dual-side polished SPR PCF sensor for ultra-wide analyte range in the visible to near-IR operating band. Optical and Quantum Electronics, (2024). 56(7): p. 1187. Available: https://link.springer.com/article/10.1007/s11082-024-07146-4

[12] Moftakharzadeh, A., B. Afkhami Aghda, and M. Hosseini, Noise Equivalent Power Optimization of Graphene-Superconductor Optical Sensors in the Current Bias Mode. Journal of Optoelectronical Nanostructures, (2018). 3(3): p. 1-12. Available: https://d1wqtxts1xzle7.cloudfront.net/94517205/article_3040_c11f2d8d2fa24f1f5bb3d07f5a0660f1-libre.pdf?1668880388=&response-content-disposition=inline%3B+filename%3DNoise_Equivalent_Power_Optimization_of_G.pdf&Expires=1756633568&Signature=QS6Z5QVxCyBDPMtbtbcF2iNdl6uZmv~I4rgg6f8xgr9oB1j1sGxNZRsLFkCG3pphtergQ2Y1-9DJcOMYk7eBG1jqSEX~iMJKRlUboyDSFun4uuF9hj4HfFtVDkDslq6F8CoTnog6t2cy44f71tVypzFPBBd4kdWXz0syB6yWooirg1R9I~dtCDutDNRxlxXKrHlj8NuyE9sCvnbbeDqMHeedAm3XsD4eeniNCCSWYZw5V2LmvuA-5-nb-XBoCsCWLQ81DACErYHZTrjM3YEGmL2iBfxsvHoRc9ceworO8F47D7Q~m-fvzKwOd7p5Km087VAgp8uSTQ0ZtgoljAD79g__&Key-Pair-Id=APKAJLOHF5GGSLRBV4ZA

[13] Mousavi Monazah, S.M., M.R. Salehi, and F. Emami, Mathematical model for highly sensitive photonic crystal fiber sensor based on hyperbolic black holes. Scientific Reports, (2024). 14(1): p. 25997. Available: https://www.nature.com/articles/s41598-024-75910-3

[14] Jing, J.-Y., Q. Wang, and B.-T. Wang, Refractive index sensing characteristics of carbon nanotube-deposited photonic crystal fiber SPR sensor. Optical fiber technology, (2018). 43: p. 137-144. Available: https://www.sciencedirect.com/science/article/abs/pii/S1068520018301512

[15] Manickam, P., R. Senthil, and R. Senthil, Numerical Analysis of Hybrid-SPR-PCF Multi-Analyte Sensor for Clinical Diagnosis. Plasmonics, (2024): p. 1-7. Available: https://link.springer.com/article/10.1007/s11468-024-02486-z

[16] Islam, M.I., et al., Design and optimization of photonic crystal fiber based sensor for gas condensate and air pollution monitoring. Photonic Sensors, (2017). 7: p. 234-245. Available: https://link.springer.com/article/10.1007/s13320-017-0404-6

[17] Manickam, P. and R. Senthil, Numerical investigation of side-polished SPR PCF sensor for urine analysis. Plasmonics, (2022). 17(5): p. 2023-2030. Available: https://link.springer.com/article/10.1007/s11468-022-01688-7

[18] Fallahi, V., Z. Kordrostami, and M. Hosseini, Cancer detection by photonic crystal optical biosensors: Effect of hexagonal micro ring resonator design. Materials Science in Semiconductor Processing, (2024). 174: p. 108188. Available: https://www.sciencedirect.com/science/article/abs/pii/S1369800124000842

[19] Kaur, V. and S. Singh, Design of titanium nitride coated PCF-SPR sensor for liquid sensing applications. Optical Fiber Technology, (2019). 48: p. 159-164. Available: https://www.sciencedirect.com/science/article/abs/pii/S1068520018304930

[20] Hossain, M.B., et al., Numerical development of high performance quasi D-shape PCF-SPR biosensor: An external sensing approach employing gold. Results in Physics, (2020). 18: p. 103281. Available: https://www.sciencedirect.com/science/article/pii/S2211379720317484

[21] Sakib, M.N., et al., High performance dual core D-shape PCF-SPR sensor modeling employing gold coat. Results in Physics, (2019). 15: p. 102788. Available:https://www.sciencedirect.com/science/article/pii/S221137971932981X

[22] Huang, T., Highly sensitive SPR sensor based on D-shaped photonic crystal fiber coated with indium tin oxide at near-infrared wavelength. Plasmonics, (2017). 12: p. 583-588. Available: https://link.springer.com/article/10.1007/s11468-016-0301-7

[23] Liu, Z. and H. Li, A high magnetic field sensitivity PCF- SPR sensor working in the near- infrared wavelength band. Microwave and Optical Technology Letters, (2024). 66(1): p. e33820. Available: https://onlinelibrary.wiley.com/doi/full/10.1002/mop.33820?casa_token=nvUykZXOvpgAAAAA%3Ace3tfwLMRKbXoefbFf11DvhrTb5JOn0dEBRs47sLrfBf-blQ9pO5RO7M8Ysjs-7x2wlbTP_PIm8jaHVtJQ

[24] Kaziz, S., F. Echouchene, and M.H. Gazzah, Optimizing PCF-SPR sensor design through Taguchi approach, machine learning, and genetic algorithms. Scientific Reports, (2024). 14(1): p. 7837. Available: https://www.nature.com/articles/s41598-024-55817-9

[25] Islam, M.R., et al., AZO-coated plasmonic PCF nanosensor for blood constituent detection in near-infrared and visible spectrum. Applied Physics A, (2022). 128(1): p. 86. Available: https://link.springer.com/article/10.1007/s00339-021-05220-2

[26] Rahman, M.H., et al., Dual-function plasmonic device on photonic crystal fiber for near to mid-infrared regions. Optical Materials Express, (2023). 13(9): p. 2526-2540. Available: https://opg.optica.org/abstract.cfm?uri=ome-13-9-2526

[27] Zuhayer, A. and A. Shafkat, Design and analysis of a gold-coated dual-core photonic crystal fiber bio-sensor using surface plasmon resonance. Sensing and Bio-Sensing Research, (2021). 33: p. 100432. Available: https://www.sciencedirect.com/science/article/pii/S2214180421000374

[28] Yu, Z., et al., High extinction ratio and large bandwidth PCF polarization filter with gold-wires coated by monocrystalline silicon. IEEE Photonics Journal, (2022). 14(4): p. 1-6. Available: https://ieeexplore.ieee.org/abstract/document/9839593

[29] Islam, M.R., et al., Peak amplitude difference sensitivity (PADS): an interrogation technique for PCF-SPR sensors using symmetrical arrays of plasmonic layers. Results in Physics, (2023). 48: p. 106434. Available:https://www.sciencedirect.com/science/article/pii/S2211379723002279

[30] Tahhan, S.R. and R.M. Taha, Mercedes Benz logo based plasmon resonance PCF sensor. Sensing and Bio-Sensing Research, (2022). 35:

p. 100468. Available: https://www.sciencedirect.com/science/article/pii/S2214180421000738

[31] Wang, Q., et al., Research advances on surface plasmon resonance biosensors. Nanoscale, (2022). 14(3): p. 564-591. Available: https://pubs.rsc.org/en/content/articlelanding/2016/jy/d1nr05400g/unauth

[32] Chauhan, M. and V.K. Singh, TiO2 coated tapered optical fiber SPR sensor for alcohol sensing application. Journal of Optics, (2023): p. 1-11. Available: https://link.springer.com/article/10.1007/s12596-023-01131-y

[33] Zhang, Q., et al., Highly sensitive surface plasmon resonance temperature sensor based on a hollow core fiber multilayer structure. Optics Express, (2023). 31(15): p. 23840-23850. Available: https://opg.optica.org/abstract.cfm?uri=oe-31-15-23840

[34] Mousavi Monazah, S.M., F. Emami, and M.R. Salehi, Design and analysis of nano gold coated refractive index sensor with asymmetric multiple holes. Plasmonics, (2023). 18(3): p. 931-940. Available: https://link.springer.com/article/10.1007/s11468-023-01823-y

[35] She, Y., et al., Surface plasmon resonance sensor based on a D-shaped hollow microstructured fiber with bimetallic film. JOSA B, (2024). 41(1): p. 90-97. Available: https://opg.optica.org/abstract.cfm?uri=josab-41-1-90

[36] Zhang, X., et al., Numerical Simulation of Optical Fiber Tamm Plasmon Polariton Sensor Based on D-shaped Hollow-core Photonic Crystal Fiber Coated with a Gold Film. IEEE Sensors Journal, (2024). Available: https://ieeexplore.ieee.org/abstract/document/10399342

[37] Monazah, S.M.M., et al., Design and numerical analysis of a highly sensitive nano-layer coated photonic crystal fiber biosensor. Laser Physics, (2023). 33(8): p. 086201. Available: https://iopscience.iop.org/article/10.1088/1555-6611/acd7db/meta

[38] Hussain, N., et al., Dual core photonic crystal fiber based plasmonic refractive index sensor with ultra-wide detection range. Optics Express,

(2023). 31(16): p. 26910-26922. Available: https://opg.optica.org/oe/abstract.cfm?uri=oe-31-16-26910

[39] Mittal, S., et al., Design and performance analysis of a novel hoop-cut SPR-PCF sensor for high sensitivity and broad range sensing applications. IEEE Sensors Journal, (2023). 24(3): p. 2697-2704. Available: https://ieeexplore.ieee.org/abstract/document/10355908